Journal of Nuclear Medicine, published on November 2, 2017 as doi:10.2967/jnumed.117.197665

Comparison of PET/CT with sequential PET/MRI using an MR-compatible mobile PET system

Ryusuke Nakamoto, Yuji Nakamoto, Takayoshi Ishimori, Yasutaka Fushimi, Aki Kido, Kaori Togashi

Department of Diagnostic Imaging and Nuclear Medicine, Kyoto University Graduate School of Medicine

Corresponding author

Yuji Nakamoto, MD, PhD

Department of Diagnostic Imaging and Nuclear Medicine, Kyoto University Graduate School of Medicine, 54 Shogoin-kawahara-cho, Sakyo-Ku, Kyoto 606-8507, Japan

E-mail: ynakamo1@kuhp.kyoto-u.ac.jp

Phone. +81-75-751-3762 Fax. +81-75-771-9709

First author

Ryusuke Nakamoto, MD (Graduate student)

Department of Diagnostic Imaging and Nuclear Medicine, Kyoto University Graduate School of Medicine, 54 Shogoin-kawahara-cho, Sakyo-Ku, Kyoto 606-8507, Japan

E-mail: inabook@kuhp.kyoto-u.ac.jp

Phone. +81-75-751-3762 Fax. +81-75-771-9709

Word count: 5,028 words

Short running title: A new MR-compatible mobile PET scanner

ABSTRACT

Objectives: The current study tested a newly developed flexible PET (positron emission tomography) scanner prototype. This flexible PET (fxPET) system involves dual arc-shaped detectors based on silicon photomultipliers, which are designed to fit existing magnetic resonance (MR) devices, allowing us to get fused PET and MR images by sequential PET scanning. This prospective study sought to evaluate image quality, lesion detection rate, and quantitative values of fxPET in comparison with conventional whole-body (WB) PET images, and to assess the accuracy of registration.

Methods: Seventeen patients with suspected or known malignant tumors were analyzed. Approximately 1 h after intravenous injection of ^{18}F-fluorodeoxyglucose (FDG), WB PET/computed tomography (CT) scanning was performed, followed by fxPET and MR scanning. For reconstruction of fxPET images, MRI-based attenuation correction was applied. The quality of fxPET images was visually assessed, and the number of detected lesions was compared between the two imaging methods. The maximum standardized

uptake values (SUVmax) and maximum average SUV within a 1 cm^3 spherical volume (SUVpeak) of lesions were also compared. In addition, the magnitude of misregistration between fxPET and MR images was evaluated.

Results: The image quality of fxPET was acceptable for diagnosis of malignant tumors. There was no significant difference in detectability of malignant lesions between fxPET and WB PET ($P > 0.05$). However, the system did not exhibit superior performance compared with WB PET. There were strong positive correlations between the two imaging modalities in SUVmax ($\rho = 0.88$) and SUVpeak ($\rho = 0.81$). SUVmax and SUVpeak measured with fxPET were approximately 1.1-fold greater compared with WB PET measurements. The average misregistration between fxPET and MR images was 5.5 ± 3.4 mm.

Conclusion: Our preliminary data indicate that running a fxPET scanner in the proximity of an existing MR system provided visually and quantitatively acceptable fused PET/MR images for diagnosis of malignant lesions.

Keywords: flexible PET scanner, mobile PET, PET/MRI, MRI

INTRODUCTION

Hybrid PET/MRI is a recent advance in multimodality imaging, providing both anatomical and functional information *(1,2)*. PET/MRI systems have several important advantages, compared with PET/CT. First, MRI is considered to be superior to CT for soft-tissue contrast, and is regarded as the first-line imaging procedure in oncology associated with soft-tissue regions (e.g., tumors in the brain, the head-and-neck region, the musculoskeletal region, and the pelvis) *(3)*. Second, MRI can yield functional information about perfusion, diffusion, and metabolism *(2)*. Third, the use of MRI instead of CT for attenuation correction reduces radiation dose, particularly in patients undergoing repeat PET studies *(4,5)*. In addition, integrated PET/MRI systems which perform simultaneous PET and MRI acquisition afford significantly more accurate registration than sequential scanning of conventional PET/CT scanners *(6)*. Precise registration between PET and

anatomic MRI is important for diagnosing pathologic conditions, avoiding errors in interpretation, surgical planning, and delineating radiation therapy margins *(6)*. PET/MRI scanners have recently been developed by several vendors, and an increasing number of studies using these systems have been published. However, PET/MRI scanners are not widely available, because the costs (including the cost of facilities) are far greater than those of PET/CT. To overcome these limitations, a multi-modal compatible prototype called the flexible PET system (fxPET) has been developed. This new device is a prototype of an MRI-compatible PET scanner with silicon photomultiplier array-based depth-of-interaction and time-of-flight capable (TOF) detectors *(7)*. This device is designed to fit existing MR devices, allowing us to get fused PET and MR images by sequential PET scanning.

The purpose of this prospective study was to evaluate image quality, lesion detection rate, and quantitative values of fxPET, compared with conventional whole-body (WB) PET imaging, and to assess the accuracy of registration.

MATERIALS AND METHODS

Patients

A total of 17 patients (nine males, eight females) with suspected or known malignant tumors who underwent fxPET scanning between February 2015 and May 2015 were analyzed. All patients underwent a dual- imaging, single-injection protocol consisting of PET/CT and subsequent fxPET/MRI on the same day. The institutional review board approved the study, and all subjects gave written informed consent.

Description of the flexible PET scanner system

The fxPET scanner consists of two detector units that enable the fitting of beds of other imaging modalities and patients of various body sizes *(8)*. The dual arc-shaped detector heads can be arranged in various configurations, including top-bottom, and left-right, depending on the purpose of imaging. The fxPET system is shown in Figure 1. Each detector unit consists of 18 detector modules in the transaxial direction and three rings in the axial direction, with a detector ring diameter of 778 mm and an axial extent of 150 mm.

The detector block is composed of four-layer depth-of-interaction crystal blocks of lutetium oxyorthosilicate crystals (Hitachi Chemical, Japan), a light guide and a 64-ch MRI-compatible silicon photomultiplier array (Hamamatsu Photonics, Japan). The coincidence timing resolution of the system is approximately 500 psec. As shown in Figure 1, the fxPET scanner is a partial-ring scanner rather than a conventional full-ring scanner, and its limited angular coverage results in missing line-of-responses in sinogram space. In practice, degradation of image quality caused by data loss due to incomplete coincidence data was confirmed by a previous phantom study, and was found to be reduced by using TOF information and more suitable list-mode reconstruction algorithms *(8,9)*. Each crystal is 20 mm long, with a cross-sectional area of 2.9 × 2.9 mm and four-layer depth-of-interaction capability. The spatial resolution of these scanners measured with an ^{18}F point source was estimated to be less than 2.5 mm. The main specifications of the fxPET system are summarized in Table 1.

Several phantom studies were conducted in preparation for the clinical study of fxPET/MRI. A National Electrical Manufacturers Association image-quality phantom study

with the fxPET scanner demonstrated that the device was able to clearly depict the smallest sphere (10 mm) *(7)*. Another preclinical study using with an MR phantom was performed to investigate whether there was an adverse influence on MR images after installation of the fxPET scanner to a 1.5 T MRI system, and detected no adverse influence on MR images *(10)*. In addition, an experimental study detected no adverse effects of the 1.5 T MRI system on fxPET images *(10)*.

Conventional PET/CT and fxPET/MRI

An intravenous injection of ^{18}F-FDG (~3.7 MBq/kg of weight) was followed by WB PET/CT scanning at 1 h post-injection, using a combined PET/CT scanner (Discovery ST Elite or Discovery IQ; GE Healthcare, Waukesha, WI, USA) for 2–3 min/bed position. Patients then underwent fxPET scanning with 10 min/bed position, followed by MR scanning for 20 min (mean 17 min; range, 10–25 min). To reduce the time needed for fxPET/MRI scanning, the scan range of fxPET was limited to one bed position (axial field-of-view [FOV] of 150 mm). Therefore, the fxPET scan range was determined according to

the site of primary tumors (the neck, upper abdomen, pelvis, or musculoskeletal region) using information from CT, MRI, and WB PET/CT findings obtained prior to fxPET scanning in this study. All fxPET scans were performed with dual arc-shaped detectors arranged in a top-bottom configuration (Fig. 1C). The central angle of the detector was 135 degrees; the detector pair covered 270 degrees out of 360 degrees (Supplemental Fig. 1). A larger MRI scan range was determined to include the whole scan range of fxPET. The mean duration between ^{18}F-FDG injection and the start of fxPET scanning was 114 min (range, 92–161 min). Table 2 summarizes the difference of acquisition conditions and system sensitivity between the fxPET and WB PET/CT systems. No patients had a plasma glucose level greater than 200 mg/dL. WB PET images were attenuation-corrected using CT data and reconstructed using a 3D ordered-subsets expectation-maximization algorithm called VUE Point Plus (Discovery ST Elite; 14 subsets, two iterations, a matrix size of 128 × 128, a voxel size of 4.7 × 4.7 × 3.3 mm, and post-filtering at 5 mm full width at half maximum; Discovery IQ; 12 subsets, four iterations, a matrix size of 192 × 192, a voxel size of 3.3 × 3.3 × 3.3 mm, and post-filtering at 5 mm full width at half maximum). All acquisition

fxPET data were reconstructed with a dynamic row-action maximum-likelihood algorithm (DRAMA) *(11)* (128 subsets, one iteration, a matrix size of 240 × 240 × 50, a voxel size of 3.0 × 3.0 × 3.0 mm, and relaxation control parameter β = 30 with post-filtering of 5 mm full width at half maximum). The MRI scanner was a 1.5 Tesla (T) MRI scanner (EXCELART Vantage; Toshiba Medical Systems Corporation, Otawara, Japan). Diagnostic MRI sequences (including T1-weighted imaging, T2-weighted imaging, T2-weighted short-tau inversion recovery, and diffusion-weighted imaging) were determined according to the site of primary tumors. In this study, we applied a newly developed method of MRI-based attenuation correction to fxPET images *(12,13)*. Conventional segmentation methods of MRI-based attenuation correction ignore the presence of bony structures and have been found to underestimate SUVs of regions containing bone or regions close to large bony structures, such as the brain and pelvis *(5)*. In contrast, the new method generates a distribution of attenuation correction factors by considering bone attenuation using diagnostic T1-weighted images. The parameters of the axial T1-weighted image were determined according to the scan site of MRI: matrix size 192–576 × 288–576, FOV 220–

350 mm × 220–500 mm, slice thickness 4.0 or 5.0 mm with 0 or 1 mm gap, TR 272–570 msec, TE 4.8-15 msec, and a flip angle of 70° or 90°. The attenuation map for the MR table was obtained using the background activity of lutetium oxyorthosilicate scintillators. The method of scatter corrections was TOF Single Scatter Simulation *(14)*.

Visual analysis

I. Evaluation of image quality. The image quality of fxPET was visually compared with that of WB PET by two board-certified nuclear medicine physicians blinded to clinical information, including other clinical images, using a 4-point grading scale: 1, poor for diagnosis; 2, acceptable for diagnosis but inferior to WB PET; 3, comparable to WB PET; 4, superior to WB PET. The degree of inter-observer agreement was evaluated using weighted Kappa statistics. Kappa values of 0.81–1.00, 0.61–0.8, 0.41–0.60, 0.21–0.40, and 0–0.2 were defined as indicating almost perfect, substantial, moderate, fair, and slight agreement, respectively *(15)*.

II. Evaluation of the lesion detection rate. The number of lesions detected on fxPET

images was compared with the number detected on WB PET images based on the final diagnosis by two board-certified nuclear medicine physicians, reached by consensus. Lesions less than 5 mm in diameter measured by CT or MR were excluded from the analysis. Focal moderate to intense uptake of ^{18}F-FDG, compared with the surrounding tissue, was regarded as positive. If lesions were so close together that PET tracer uptake of lesions could not be individually distinguished, it was counted as one lesion. The gold standard for the final diagnosis was histopathological findings (biopsy or surgery), or serial radiological follow-up (CT and/or MRI and/or WB PET/CT) revealing further metastatic lesions, or, alternatively, the disappearance of metastatic lesions following systemic therapy or clinical follow up for at least 6 months *(16)*. Both fxPET and WB PET images were evaluated using the Osirix MD (Pixmeo, Geneva, Switzerland).

Quantitative analysis

The maximum standardized uptake values (SUVmax) and maximum average SUV within a 1 cm^3 spherical volume (SUVpeak) of lesions were measured for both fxPET

and WB PET images *(17)*. The SUVmax and SUVpeak were only available for lesions that met the gold standard, were entirely within the FOV, and could be visually detected on both fxPET and WB PET images (n = 28). Pulmonary lesions and lesions containing wide lung fields in the same axial cross section were excluded, because the MRI-based attenuation correction method did not take account of attenuation of lung fields.

Registration accuracy

To obtain accurate registration, image fusion of fxPET and MRI was performed using software in combination with 3D positional information obtained from an optical Polaris camera (Northern Digital Inc., Bakersfield, CA, USA). This optical tracking system provides real-time measurement data of accurate 3D position and orientation tracking of markers attached to the surface of both modalities for accurate image fusion (Fig. 2). Before the clinical study, a phantom study using a water phantom and point sources was performed to evaluate image registration accuracy. The results revealed that the average misregistration between fxPET and MR images was approximately 2 mm.

In the clinical study, the registration accuracy of clinical fxPET/MR images was retrospectively evaluated by one observer using the above-mentioned fusion software (Osirix MD). The spatial coordinates (X, Y, Z) of the visually estimated centers of the lesions were determined for fxPET/MRI (i.e., for fxPET and MR images independently) by calculating the middle slice for each section for all three planes *(18)*. The coordinate differential in the three axes was determined, and Delta X was defined as coordinate X axis fxPET - coordinate X axis MRI. The same process was used for the Y and Z axes. The total difference between the lesion centers on fxPET and MRI was determined by the following formula: Difference = $(\text{Delta X}^2+\text{Delta Y}^2+\text{Delta Z}^2)^{0.5}$ *(19)*. The same 28 lesions included in the quantitative analysis were analyzed. To avoid inaccurate measurement, six lesions from a case in which a patient was unable to remain still during fxPET/MRI examination were excluded from the analysis. One lesion in which FDG uptake was not sufficiently homogeneous to visually determine boundaries of FDG uptake was also excluded. Thus, a total of 21 lesions were finally evaluated for the extent of misregistration on fxPET/MR images.

Statistical analysis

The sensitivities of fxPET and WB PET images for lesion detection were compared with the final diagnosis using McNemar's test. Spearman's rank correlation coefficient (ρ) was calculated to assess the correlation of SUVmax and SUVpeak obtained from malignant lesions between the two scanners. A *P*-value less than 0.05 was considered to indicate statistical significance. GraphPad Prism version 6 for Windows (GraphPad Software, San Diego, CA, USA) and Excel 2016 (Microsoft, Redmond, WA, USA) were used for statistical analysis.

RESULTS

Patient characteristics, including the results of the visual analysis, are shown in Table 3. Figure 3 shows a representative case of fxPET/MRI.

The median ratings of visual assessment of fxPET image quality by the two observers were both grade 2 (acceptable for diagnosis but inferior to WB PET). The weighted Kappa score for the quantitative scales between the two observers for the quality of fxPET images was "substantial" (0.653, 95 % CI: 0.021–1.000).

A total of 41 malignant lesions (primary tumors, metastatic lymph nodes and distant metastases) were detected based on the gold standard. Of these, 35 malignant lesions (85%) were detected by fxPET, and 36 lesions (88%) were detected by WB PET. There was no significant difference in detectability of malignant lesions between fxPET and WB PET ($P > 0.05$). In addition, there were no false positive findings in both PET studies in this population.

There were strong positive correlations in SUVmax ($\rho = 0.88$) and SUVpeak ($\rho = 0.81$) between fxPET and WB PET (Fig. 4). The fxPET scanner exhibited 1.1-fold greater SUVmax and SUVpeak than WB PET/CT.

The average misregistration of the center of lesions measured with fxPET and MRI was 5.5 ± 3.4 mm for all lesions (Table 4). Misregistration was not consistent, but was more pronounced in the Z-axis (3.3 ± 2.5 mm) than the X-axis (1.3 ± 1.1 mm) and Y-axis (2.5 ± 1.7 mm).

DISCUSSION

The results of the visual analysis indicated that the fxPET system produced images of acceptable quality for diagnosis of malignant lesions. In addition, the detectability of malignant lesions was not significantly different between fxPET and WB PET images ($P > 0.05$). This is the first clinical study to evaluate the feasibility of an MRI-compatible mobile PET system, indicating that PET images would be less expensively fused to MR images which have higher soft-tissue contrast and more functional information. This system is considered helpful for reducing radiation dose, compared to PET/CT, especially when repeated scans are necessary.

The image quality of fxPET was not better than that of WB PET, although we took longer acquisition time for fxPET scanning (10 vs. 2-3 min/bed). The most likely cause of the lack of superior performance was the degradation of image quality caused by incomplete coincidence data derived from the partial-ring detector. Suri et al. reported that accurate TOF information improved reconstruction image quality in a partial-ring PET scanner with no detector rotation *(8, 9)*. Therefore, the technology of TOF was added to the fxPET system to improve image quality, although the image quality of fxPET was not superior to that of commercial WB PET scanners without TOF capability in this study. Another potential explanation is that the reconstruction conditions of fxPET images may not have been sufficiently optimized. To further improve image quality, data pre-processing and reconstruction methods dedicated to the partial-ring TOF PET are now under development.

The SUVmax and SUVpeak of lesions obtained with fxPET were 1.1-fold greater than those of WB PET/CT. Several factors may have contributed to the difference in SUVs between the two scanners. First, different duration time after administration of PET tracers

(59 min vs. 114 min) may have influenced the difference in SUVs, because the radioactive uptake of a lesion has been reported to continue increasing after injection in many cases *(20,21)*. Thus, a longer uptake phase could result in the overestimation of quantitative values of malignant lesions on fxPET images rather than underestimation. Second, fxPET images were reconstructed without taking account of attenuation from MR coils. The fact may have contributed to decrease SUVs of lesions on fxPET images. Third, attenuation correction for the MR table may have been inaccurate, because the materials of the MR table were unknown. Finally, data loss due to incomplete coincidence data obtained from the dual arc-shaped detectors arranged in a top-bottom configuration may have caused degradation of quantitative accuracy, although fxPET images were reconstructed using TOF information to reduce the effects of incomplete projection data. The difference between CT-based and MR-based attenuation correction was unlikely to have affected the difference of SUVs between the two scanners in this study, because a newly developed method of attenuation correction that takes attenuation of bony structures into account was applied on fxPET images.

The average misregistration between fxPET and MR images was 5.5 mm, and the performance of the system in the clinical study was inferior to that in the phantom study (by approximately 2 mm). The cause of the discrepancy between the two results may be related to the effects of physiological organ motion, such as respiratory motion and intestinal peristalsis, caused by the different acquisition timing between fxPET and MR imaging *(18)*. Rakheja et al. reported that the average misregistration of a hybrid PET/MRI between PET and T1-weighted MR imaging was 2.4 mm *(6)*. Their PET/MRI system exhibited more accurate spatial registration than the system in the current study. A possible explanation for this difference is that their PET/MRI system was able to perform simultaneous acquisition, whereas the current system required PET and MRI data to be collected sequentially. Nevertheless, our data suggested that acceptably accurate fused fxPET/MRI images were obtained from the current system, comparable with the lesion misregistration reported in PET/CT images in previous studies (4.1 ± 4.2 mm) *(6)*.

This pilot study revealed that our prototype of mobile PET system had several problems to be solved in order to improve its performance. Nevertheless, we consider that

the fxPET scanner would be one of the attractive imaging tools, especially from the aspect of cost. In any facilities where a state-of-art MR system is installed, fused images of PET and MR can be obtained at low cost, although the scanning is not simultaneous, but sequential. Also, due to wide inner diameter of the fxPET system, standard radiofrequency coils in MR scanning could be used in this system if we prepare CT attenuation map of them and incorporate it into the reconstruction of fxPET images. For this reason, it is not necessary to prepare dedicated radiofrequency coils for combined PET/MR. In addition, this system could be installed for other devices, such as CT or radiation therapy equipment.

The current study involved several limitations that should be considered. First, the number of enrolled patients was relatively small (n = 17). A prospective study with a larger number of patients is warranted to clarify the clinical impact of the fxPET scanner. Second, although 3T MRI is now becoming the clinical standard, this pilot study was performed with a 1.5T MRI system. It is physically feasible to install the fxPET system in close proximity to a 3T MRI system, and further studies are needed to confirm whether combined fxPET and a 3T MRI system could provide high-quality fused PET/MR images without any PET and MRI

artifacts. Third, because of the relatively long acquisition time of fxPET (10 min/bed), the scan range of fxPET/MRI was limited to only one bed position (axial FOV, 150 mm). To widen the scan range of fxPET/MRI, we plan to evaluate the extent to which we can shorten acquisition time of fxPET without degrading the quality of fxPET images using list-mode fxPET data. Because the spatial resolution of the fxPET scanner is high (full width at half maximum < 2.5 mm), we expect that the detectability of small lesions (e.g., lymph node metastases) would be improved, compared with a conventional PET scanner.

CONCLUSION

Our preliminary data indicate that a fxPET scanner placed in the proximity of an existing MR system provided visually and quantitatively acceptable fused PET/MR images for the diagnosis of malignant lesions.

ACKNOWLEDGEMENTS

We thank Kyoko Takakura, RT, for her excellent clinical assistance; Yoshiyuki Yamakawa, Masafumi Furuta, Masanobu Satoh, Tetsuya Kobayashi, Junichi Ohi, and Keishi Kitamura for their technical advice. We obtained financial support from Shimadzu Corporation, Kyoto, Japan. This study was based on results obtained from a project commissioned by the New Energy and Industrial Technology Development Organization (NEDO).

REFERENCES

1. Minamimoto R, Levin C, Jamali M, et al. Improvements in PET Image quality in time of flight (TOF) simultaneous PET/MRI. *Mol Imaging Biol.* 2016;18:776-781.

2. Pichler BJ, Kolb A, Nagele T, Schlemmer HP. PET/MRI: paving the way for the next generation of clinical multimodality imaging applications. *J Nucl Med.* 2010;51:333-336.

3. Drzezga A, Souvatzoglou M, Eiber M, et al. First clinical experience with integrated whole-body PET/MR: comparison to PET/CT in patients with oncologic diagnoses. *J Nucl Med.* 2012;53:845-855.

4. Chawla SC, Federman N, Zhang D, et al. Estimated cumulative radiation dose from PET/CT in children with malignancies: a 5-year retrospective review. *Pediatr Radiol.* 2010;40:681-686.

5. Varoquaux A, Rager O, Poncet A, et al. Detection and quantification of focal uptake in head and

neck tumours: (18)F-FDG PET/MR versus PET/CT. *Eur J Nucl Med Mol Imaging.* 2014;41:462-475.

6. Rakheja R, DeMello L, Chandarana H, et al. Comparison of the accuracy of PET/CT and PET/MRI spatial registration of multiple metastatic lesions. *AJR Am J Roentgenology.* 2013;201:1120-1123.

7. Yamakawa Y, Kobayashi T, Furuta M, et al. Development of a dual-head mobile DOI-TOF PET system having multi-modality compatibility. *in Conf. Rec. IEEE NSS/MIC*, 2014:1-3

8. Kobayashi T, Kitamura K. Design considerations for a partial-ring, multi-modal compatible whole-body TOF PET scanner: Flexible PET. *in Conf. Rec. IEEE NSS/MIC*, 2012:2807-2812.

9. Surti S, Karp JS. Design considerations for a limited angle, dedicated breast, TOF PET scanner. *Phys Med Biol.* 2008;53:2911-2921.

10. Furuta M, Satoh M, Ohi J, et al. Development of a proof of concept system for multi-modal compatible PET: Flexible PET. *in Conf. Rec. IEEE NSS/MIC*, 2013:1-4

11. Nakayama T, Kudo H. Derivation and implementation of ordered-subsets algorithms for list-mode PET data. *in Conf. Rec. IEEE NSS/MIC*, 2005;4:5.

12. Kawaguchi H, Obata T, Sano H, et al. A hybrid-segmentation atlas method to construct the attenuation correction factor for human pelvic PET/MRI. *Proc Intl Soc Mag Reson Med*. 2016;24:2186.

13. Tanigawa A, Yamaya T, Kawaguchi H, et al. Hybrid segmentation-atlas method for PET-MRI attenuation correction. *in Conf. Rec. IEEE NSS/MIC*, 2012:2727-2729

14. Watson C. Extension of single scatter simulation to scatter correction of time-of-flight PET. *IEEE Trans on Nucl Sci*. 2007;54:1679-1686.

15. Kundel HL, Polansky M. Measurement of observer agreement 1. *Radiology.* 2003;228:303-308.

16. Ali TFT. Usefulness of PET–CT in the assessment of suspected recurrent colorectal carcinoma. *The Egyptian Journal of Radiology and Nuclear Medicine.* 2012;43:129-137.

17. Boellaard R, Delgado-Bolton R, Oyen WJ, et al. FDG PET/CT: EANM procedure guidelines for tumour imaging: version 2.0. *Eur J Nucl Med Mol Imaging.* 2015;42:328-354.

18. Nakamoto Y, Tatsumi M, Cohade C, Osman M, Marshall LT, Wahl RL. Accuracy of image fusion of normal upper abdominal organs visualized with PET/CT. *Eur J Nucl Med Mol Imaging.* 2003;30:597-602.

19. Cohade C, Osman M, Marshall LN, Wahl RN. PET-CT: accuracy of PET and CT spatial registration of lung lesions. *Eur J Nucl Med Mol Imaging.* 2003;30:721-726.

20. Basu S, Alavi A. Partial volume correction of standardized uptake values and the dual time point in FDG-PET imaging: should these be routinely employed in assessing patients with cancer? *Eur J Nucl Med Mol Imaging*. 2007;34:1527-1529.

21. Nakamoto Y, Ishimori T, Sano K, et al. Clinical efficacy of dual-phase scanning using 68 Ga-DOTATOC-PET/CT in the detection of neuroendocrine tumours. *Clinical radiology*. 2016;71:1069. e1061-1069. e1065.

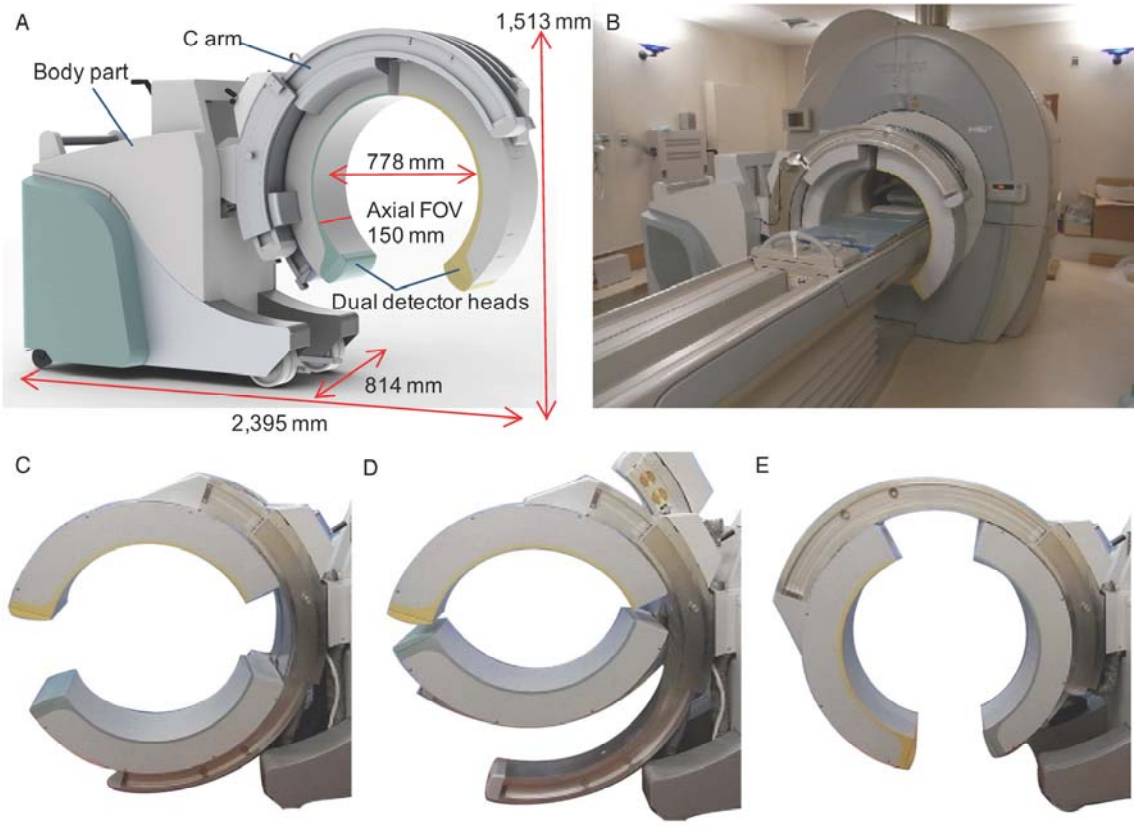

FIGURE 1. Appearance of the fxPET scanner (A-E). The device is designed to fit an existing MRI system (B). The dual arc-shaped detector heads can be arranged in various configurations: top-bottom (C), top-bottom (near-mode) (D), and left-right (E), depending on the purpose of imaging.

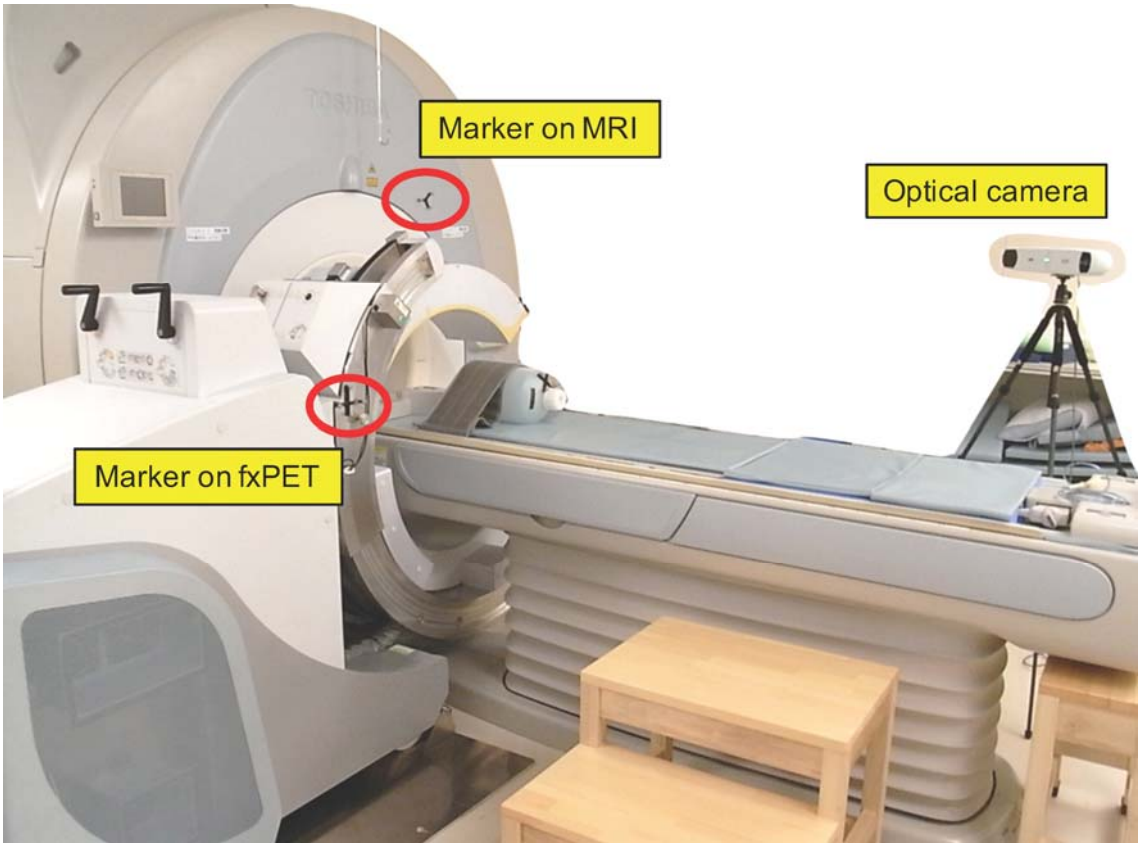

FIGURE 2. The method of fxPET/MRI image registration. The spatial registration of fxPET/MRI was performed with an optical camera measuring positional information of markers (red circles) labeled on the surfaces of both imaging modalities.

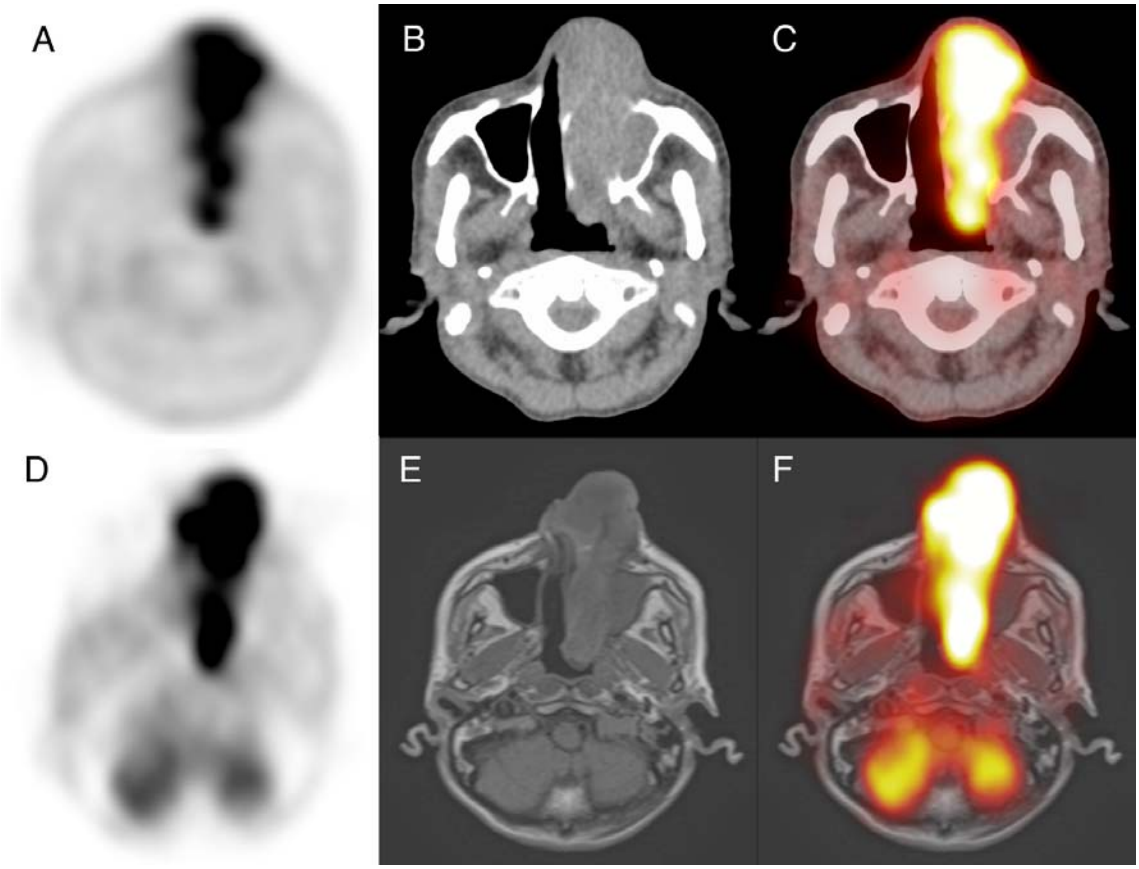

FIGURE 3. A representative case of a 76-year-old male with histologically proven nasal mucosal melanoma in his left nasal cavity. A ^{18}F- fluorodeoxyglucose (FDG) PET/CT scan (A-C), including PET (A), CT (B), and fused PET/CT images (C), shows the left nasal tumor with focal intense uptake of ^{18}F-FDG. A fxPET/MR scan (D-F), including PET (D), MR (E: T1-weighted image), and fused fxPET/MR images, also depicts the tumor clearly.

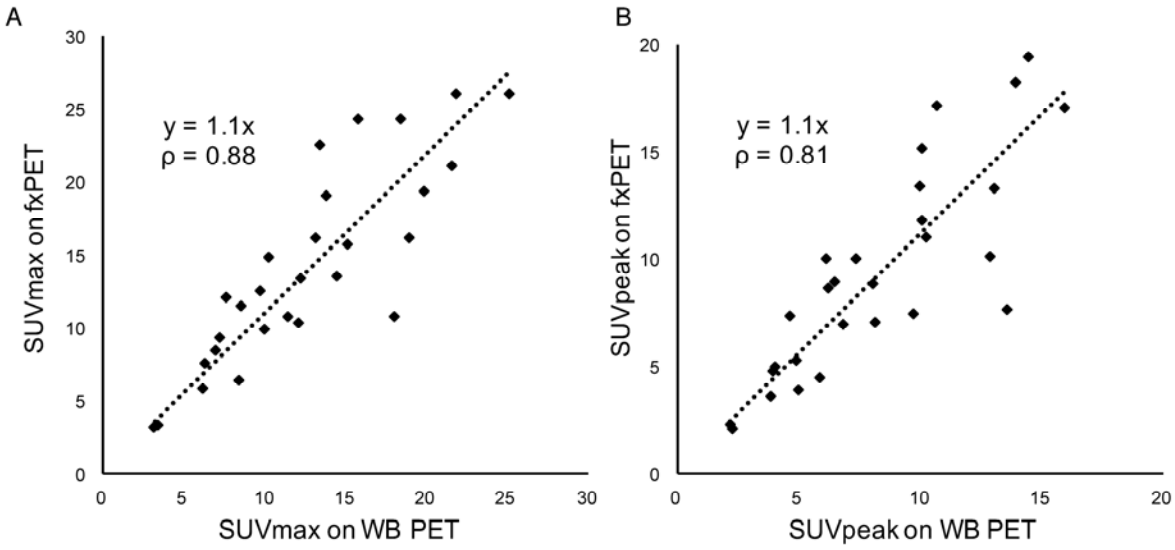

FIGURE 4. Correlations of the maximum standardized uptake values (SUVmax) and maximum average SUV within a 1 cm^3 spherical volume (SUVpeak) of 28 lesions between whole-body (WB) PET and fxPET.

TABLE 1. Specifications and characteristics of the flexible PET scanner

System description	Description value
Crystal material	LGSO ($Lu_{1.8}Gd_{0.2}SiO_5$:Ce)
Crystal size (mm^3)	2.9 × 2.9 ×20
Crystal block	Four layers of 16 × 16 arrays (256 crystal elements)
No. of detector block modules	108 (18 modules × 3 rings × 2 heads)
No. of crystals	27,648
Detector ring diameter (mm)	778
Axial FOV (mm)	150
Transaxial FOV (mm)	720
Energy resolution (%)	12.8
Temporal resolution of time-of-flight (ps)	500
Spatial resolution (mm)	< 2.5

FOV, field-of-view; LGSO, lutetium oxyorthosilicate

TABLE 2. The difference of acquisition conditions and system sensitivity between the flexible PET and whole-body PET/CT systems.

	fxPET	Discovery STE	Discovery IQ
Timing of start after FDG injection	114 min (92 min - 161 min)	58 min (49 min - 67 min)	60 min (54 min - 68 min)
Acquisition time	10 min/bed	2-3 min/ bed	2-3 min/bed
Sensitivity (the center)	2.98 cps/kBq	9.0 cps/kBq	19.44 cps/kBq
Time of flight technology	Available	Not available	Not available
Spatial resolution (mm)	< 2.5*	< 6.7	< 6.2

FDG, fluorodeoxyglucose

* Based on the iterative PSF (point spread function) reconstruction algorithm.

1 **TABLE 3.** Patient characteristics and results of visual analysis.

No.	Site	Sex	Age	Disease	Time duration between FDG injection and starting time of scanning (min)		Image quality 4-point grading scale		The number of detected lesions		
					WB PET	fxPET	Reader 1	Reader 2	Gold standard	WB PET	fxPET
1	Neck	M	46	Bone tumor	52	96	2	2	3	3	3
2		M	59	Malignant lymphoma	58	110	2	2	8	7	6
3		M	66	Tongue ca.	50	92	2	2	1	1	1
4		M	76	Melanoma	54	121	2	2	2	2	2
5	Upper abdomen	F	65	Ovarian ca.	64	126	2	2	0	0	0
6		M	70	Pancreatic ca.	50	106	2	2	1	1	1
7		M	74	HCC	62	99	2	2	1	1	1
8		M	77	Cholangiocarcinoma	62	104	2	2	5	4	4
9		F	62	pNET	58	101	2	2	1	1	1
10		F	77	pNET	49	111	2	2	4	1	1
11	Pelvis	F	66	Endometrioid ca.	62	108	3	3	4	4	4
12		F	30	Uterine cervical ca.	67	115	2	1	1	1	1
13		F	68	Uterine cervical ca.	66	132	2	2	6	6	6
14		F	52	Uterine cervical ca.	60	103	2	2	1	1	1
15		M	62	Rectal ca.	68	129	2	2	1	1	1
16	Musculoskeletal	M	73	Soft tissue sarcoma	64	126	2	2	1	1	1
17		F	39	Soft tissue sarcoma	60	161	2	2	1	1	1
	Total (n = 17)	M 9, F 8	Mean ± SD 62.5 ± 13.6		Mean ± SD 59.2 ± 6.2	Mean ± SD 114.1 ± 17	Median 2	Median 2	41	36	35

2 FDG, fluorodeoxyglucose; HCC, hepatocellular carcinoma; pNET, pancreatic neuroendocrine tumor; WB, whole-body.

TABLE 4. Difference (in mm) between the registrations of lesion center measured in three axes with fxPET and MRI

Axis	n = 21
X	1.3 ± 1.1
Y	2.5 ± 1.7
Z	3.3 ± 2.5
Total	5.5 ± 3.4

Values are mean ± SD (mm)

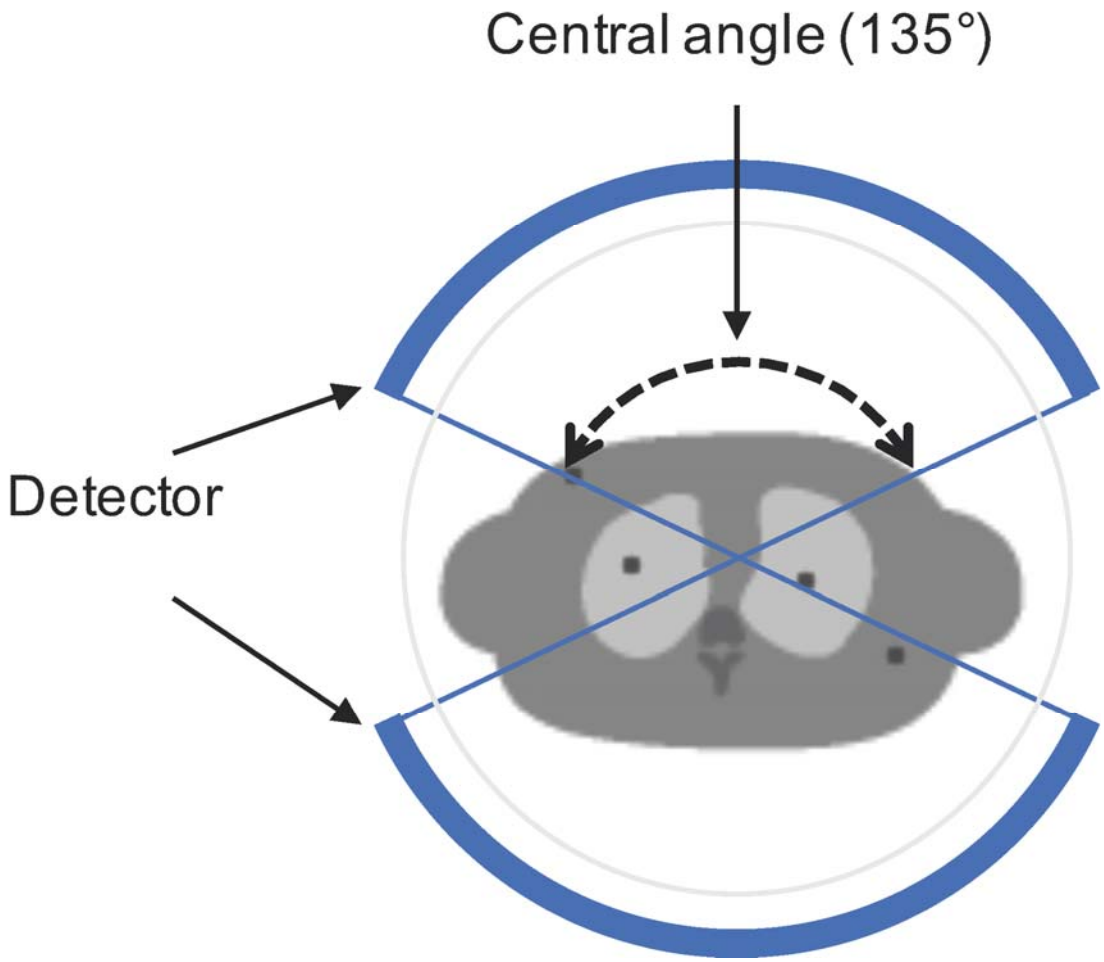

Supplemental Figure 1.

The central angle of the detector arc. The detector pair covered 270 degrees out of 360 degrees.

The Journal of NUCLEAR MEDICINE

Comparison of PET/CT with sequential PET/MRI using an MR-compatible mobile PET system

Ryusuke Nakamoto, Yuji Nakamoto, Takayoshi Ishimori, Yasutaka Fushimi, Aki Kido and Kaori Togashi

J Nucl Med.
Published online: November 2, 2017.
Doi: 10.2967/jnumed.117.197665

The Journal of Nuclear Medicine is published monthly.
SNMMI | Society of Nuclear Medicine and Molecular Imaging
1850 Samuel Morse Drive, Reston, VA 20190.
(Print ISSN: 0161-5505, Online ISSN: 2159-662X)

SNMMI SOCIETY OF NUCLEAR MEDICINE AND MOLECULAR IMAGING